Quest for Second-Harmonic-Generation-Active Coordination Polymers: Synthesis and Properties of Silver(I) Pyrimidinolates

S. Galli,*[,†] N. Masciocchi,[†] E. Cariati,[‡] A. Sironi,[§] E. Barea,*[,||] M. A. Haj,[⊥] J. A. R. Navarro,[||] and J. M. Salas[||]

Dipartimento di Scienze Chimiche e Ambientali, Università dell'Insubria, Via Valleggio 11, 22100 Como, Italy, Dipartimento di Chimica Inorganica Metallorganica ed Analitica and Dipartimento di Chimica Strutturale e Stereochimica Inorganica, Università di Milano and Istituto di Scienze e Tecnologie Molecolari del CNR (ISTM-CNR), Via Venezian 21, 20133 Milano, Italy, Departamento de Química Inorgánica, Universidad de Granada, Av. Fuentenueva S/N, 18071 Granada, Spain, and Department of Chemistry and Chemical Technology, Al Quds University, Jerusalem, Palestine

Received April 6, 2005. Revised Manuscript Received June 6, 2005

In the search for coordination compounds showing significant second harmonic generation (SHG) activity, reaction of Ag(I) ions with the 4-hydroxypyrimidine (4-Hpymo) and 5-nitro-2-hydroxypyrimidine (HNP) ligands generated four *crystalline* 1D polymers, Ag(4-pymo)·nH$_2$O (n = 2.5, 0), Ag(NP)(NH$_3$), and Ag(NP), the latter two crystallizing in acentric space groups. Their synthesis, complete characterization, and structural determination, by conventional single-crystal and laboratory X-ray powder diffraction methods, are presented and discussed in the frame of diazaaromatic-ligand- and metal-containing species. XRPD has also allowed the detection of the polyhydrated, *elusive* Ag(4-pymo)·nH$_2$O (n = 2, 3) species. Powders of Ag(NP) have shown an SHG activity close to that of standard urea. By applying the geometrical model proposed by Zyss, it is shown that the NP ligand is a highly promising chromophore, the oxo and nitro functionalities cooperatively promoting a high hyperpolarizability.

Introduction

The recent years have witnessed the blooming of coordination metal network engineering as well as the development of new topological descriptors, required by the intrinsic complexity of the polydimensional nature of the obtained materials.[1] However, in several cases, an adequate characterization of their functionality (which can range from heterogeneous catalysis,[2] magnetism,[3] optical properties,[4] sorption,[5] and even pharmaceutical[6] applications) is still missing.

Recently, we have focused our attention on a number of three-dimensional copper polymers (sodalitic metal−organic frameworks, MOFs), based on the pyrimidinol-*X*-ate ligands (*X*-pymo, X = 2 or 4; see Chart 1), which showed very interesting, reversible, (often selective) sorptive properties with a number of gases, liquids, and even ion pairs.[7] When other 3d-transition-metal ions were employed, unprecedented polymer topologies were discovered [e.g., Zn(4-pymo)$_2$[8]], molecular magnets prepared [e.g., Co(2-pymo)$_2$[9]], or species stable, upon thermal treatment, up to 500 °C found [e.g., Zn(2-pymo)$_2$[10]]. In the latter study, where only the 2-pymo ligand was used, the isolation of noncentrosymmetric crystals prompted us to test them as second-harmonic-generation (SHG)-active materials. Disappointingly, their SHG efficiency, measured by the powder Kurtz−Perry method,[11] fell in the range of a few percent of that of standard urea.

Chart 1

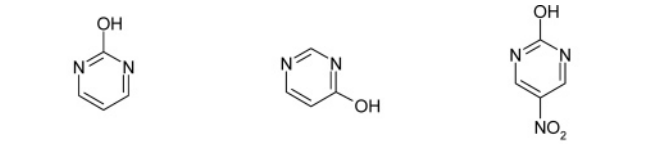

pyrimidin-2-ol (2-Hpymo) pyrimidin-4-ol (4-Hpymo) 5-nitro-pyrimidin-2-ol (HNP)

[†] Università dell'Insubria.
[‡] Dipartimento di Chimica Inorganica Metallorganica ed Analitica, Università di Milano and ISTM-CNR.
[§] Dipartimento di Chimica Strutturale e Stereochimica Inorganica, Università di Milano and ISTM-CNR.
[||] Universidad de Granada.
[⊥] Al Quds University.

(1) Blatov, V. A.; Carlucci, L.; Ciani, G.; Proserpio, D. M. *Cryst. Eng. Commun.* **2004**, *6*, 377 and references therein.
(2) Fujita, M.; Kwon, Y. I.; Washizu, S.; Ogura, K. *J. Am. Chem. Soc.* **1994**, *116*, 1152.
(3) Kahn, O.; Jay, C. *Science* **1998**, *279*, 44.
(4) (a) Burini, A.; Bravi, R.; Fackler, J. P., Jr.; Galassi, R.; Grant, T. A.; Omary, M. A.; Pietroni, B. R.; Staples, R. J. *Inorg. Chem.* **2000**, *39*, 3158 and references therein. (b) Yang, G.; Raptis, R. G. *Inorg. Chem.* **2003**, *42*, 261.
(5) See, e.g.: (a) Maji, T. K.; Uemura, K.; Chang, H.-C.; Matsuda, R.; Kitagawa, S. *Angew. Chem.* **2004**, *43*, 3269. (b) Rosi, N. L.; Eckert, J.; Eddaoudi, M.; Vodak, D. T.; Kim, J.; O'Keeffe, M.; Yaghi, O. M. *Science* **2003**, *300*, 1127. (c) Chae, H. K.; Siberio-Perez, D. Y.; Kim, J.; Go, Y.; Eddaoudi, M.; Matzger, A. J.; O'Keeffe, M.; Yaghi, O. M. *Nature* **2004**, *427*, 523.
(6) Nomiya, K.; Tsuda, K.; Sudoh, T.; Oda, M. *J. Inorg. Biochem.* **1997**, *68*, 39.
(7) (a) Tabares, L. C.; Navarro, J. A. R.; Salas, J. M. *J. Am. Chem. Soc.* **2001**, *123*, 383. (b) Barea, E.; Navarro, J. A. R.; Salas, J. M.; Masciocchi, N.; Galli, S.; Sironi, A. *Polyhedron* **2003**, *22*, 3051. (c) Barea, E.; Navarro, J. A. R.; Salas, J. M.; Masciocchi, N.; Galli, S.; Sironi A. *J. Am. Chem. Soc.* **2004**, *126*, 3014 and references therein.
(8) Barea, E.; Navarro, J. A. R.; Salas, J. M.; Masciocchi, N.; Galli, S.; Sironi, A. *Inorg. Chem.* **2004**, *43*, 473.
(9) Masciocchi, N.; Galli, S.; Sironi, A.; Barea, E.; Navarro, J. A. R.; Salas, J. M.; Tabares, L. C. *Chem. Mater.* **2003**, *15*, 2153.
(10) Masciocchi, N.; Ardizzoia, G. A.; La Monica, G.; Maspero, A.; Sironi, A. *Eur. J. Inorg. Chem.* **2000**, 2507.
(11) Kurtz, S. K.; Perry, T. T. *J. Appl. Phys.* **1968**, *39*, 3798.

10.1021/cm050739d CCC: $30.25
Published on Web 08/26/2005

Aiming to prepare more efficient SHG materials, we decided to employ different metals and differently substituted pyrimidinolate-based ligands, trying to resort to distinct electronic properties and steric requirements. As for the ligands, we shifted to 4-pymo, a constitutional isomer of 2-pymo, differing in the position of the exocyclic oxygen (Chart 1). Concomitantly, prompted by the recent appearance of scientific reports on the suitability, for significant SHG activity, of molecular species of C_{2v} symmetry,[12] we decided to prepare a highly polarized 2-pymo derivative, 5-nitro-2-pyrimidinolate (NP; see Chart 1), using one of the most efficient electron-attractor substituents.

Within this ligand, in its deprotonated form, the oxo and nitro functionalities, in *para* positions to each other, are likely to favor, by a synergic mechanism, the formation of a significant dipole moment, thus enhancing, according to the "two-level model",[13] the first hyperpolarizability. Indeed, its formal (Hammett's) $\Delta\sigma_P$ value [$\sigma_P(NO_2) - \sigma_P(O^-) = +0.78 - (-0.52) = +1.30$] is among the largest which can be computed for 1,4-disubstituted benzenes.[14] Moreover, in agreement with Dewar's rules,[15] the insertion of an electron-attractor group (NO_2 in the present case) at the *para* position of a donor group (O^-) implies a hypsochromic shift of the electronic absorption band with respect to the unsubstituted heterocycle, the NP ligand thus granting the optical transparency already offered by the parent 2-pymo.

Unfortunately, the use of these new ligands with a number of M(II) ions [M(II) = Co, Ni, and Zn][8,9,16] resulted in centrosymmetric materials, thus vanishing our initial efforts. Accordingly, we turned to M(I) ions, which are prone to digonal coordination of *N*,*N*′-*exo*-bidentate ligands and afford 1D polymers[17] and folded helices.[18] An important requirement in view of its possible applications is the transparency of the SHG material in a vast spectral range, to avoid absorption of the second harmonic produced. Silver [and often even Cu(I)] typically affords colorless materials, thus being the metal of choice from the point of view of the SHG efficiency−transparency tradeoff.

Thus, in the following, we report on the synthesis, characterization, and structural determination, by conventional single-crystal and laboratory X-ray powder diffraction methods, of four new Ag(I) polymeric species (containing the 4-pymo or the NP ligand), the structural and optical properties of which are discussed in the frame of diazaaromatic-ligand- and metal-containing species, recently reviewed by us.[19]

Experimental Section

Instrumentation and Methods. Pyrimidin-4-ol (4-Hpymo), supplied by Aldrich Chemical Co., was used as received. 5-Nitropyrimidin-2-ol (HNP) was prepared according to literature methods.[20] The other chemical reagents and solvents were supplied by commercial sources. Microanalyses of C, H, and N were performed with a Fisons-Carlo Erba EA 1008 analyzer. Thermogravimetric and differential scanning calorimetric analyses were performed, under a reactive atmosphere of air, on Shimadzu-TGA-50H/DSC equipment, at heating rates of 20 and 10 °C min^{-1}, respectively (Scientific Instrumentation Center of the University of Granada). IR spectra were recorded in the 4000−300 cm^{-1} range on a ThermoNicolet IR 200 using KBr pellets.

Synthesis of 1−4. *Preparation of [Ag(4-pymo)·2.5H$_2$O]$_n$, **1**.* An ammonia/water (1:10) solution (25 mL) containing pyrimidin-4-ol (4 mmol) was added dropwise into an ammonia/water (1:10) solution (15 mL) of $AgNO_3$ (2 mmol). The resulting colorless solution afforded a white microcrystalline material of [Ag(4-pymo)·mH$_2$O]$_x$ formulation. Single crystals of **1** suitable for X-ray diffraction studies were obtained upon drying a water suspension of [Ag(4-pymo)·mH$_2$O]$_x$ in air. Yield: 80%. Anal. Calcd for $C_4H_8N_2O_{3.5}Ag$: C, 19.37; H, 3.25; N, 11.30. Found: C, 19.5; H, 3.3; N, 11.4. IR (selected bands in cm^{-1}): 3380 vs, 1629 vs, 1556 s, 1481 vs, 1425 vs, 1362 m, 1335 m, 1200 w, 1162 w, 1008 m, 877 m, 842 s, 673 m, 602 m, 540 m.

*Preparation of [Ag(4-pymo)]$_n$, **2**.* **2** can be prepared by controlled thermal treatment of **1**. Compound **1** (25 mg) was heated at 200 °C for 20 min. In this way, the anhydrous crystalline phase **2** was obtained. Yield: 100%. Anal. Calcd for $C_4H_3N_2OAg$: C, 23.67; H, 1.49; N, 13.80. Found: C, 23.9; H, 1.5; N, 13.9. IR (selected bands in cm^{-1}): 1603 s, 1363 s, 1331 s, 1066 m, 841 m.

*Preparation of [Ag(NP)(NH$_3$)]$_n$, **3**.* **3** was synthesized following a procedure similar to that of **1**. In this case, only microcrystalline powders were obtained, which were filtered off and dried in air. Yield: 70%. Anal. Calcd for $C_4H_5N_4O_3Ag$: C, 18.13; H, 1.90; N, 21.14. Found: C, 18.1; H, 1.8; N, 20.5. IR (selected bands in cm^{-1}): 3424 m, 1653 m, 1591 vs, 1549 vs, 1389 s, 1336 vs, 1294 s, 1161 m, 829 m, 800 m, 743 m, 681 m. That NH_3, and not H_2O, is present in this species is supported by the elemental analysis and by the observation that **3** is not formed in the absence of ammonia, and that, upon suspending it in water, the anhydrous species [Ag(NP)]$_n$, **4**, is quantitatively formed (see below); in fact, the broad IR band falling slightly above 3400 cm^{-1} does not help in uniquely assigning the correct stretching mode, nor can XRPD discriminate between the two isoelectronic and nearly isosteric molecules. The material is nearly colorless and presents MLCT UV absorption bands near 340 nm.

*Preparation of [Ag(NP)]$_n$, **4**.* Thermal treatment of **3** by heating over 175 °C led to the isolation of **4**. This anhydrous phase can also be obtained by suspension of **3** in water, posterior filtration, and leaving the product recovered to dry in air. Yield: 100%. Anal. Calcd for $C_4H_2N_3O_3Ag$: C, 19.38; H, 0.81; N, 16.95. Found: C, 19.5; H, 1.1; N, 16.8. IR (selected bands in cm^{-1}): 1640 s, 1625 s, 1590 vs, 1550 vs, 1421 m, 1387 m, 1337 vs, 1312 vs, 1282 s,

(12) (a) Moylan, R.; Ermer, S.; Lovejoy, S. M.; McComb, I.-H.; Leung, D. S.; Wortmann, R.; Krdmer, P.; Twieg, R. J. *J. Am. Chem. Soc.* **1996**, *118*, 12950. (b) Le Bozec, H.; Renouard, T. *Eur. J. Inorg. Chem.* **2000**, 229.
(13) (a) Oudar, J. L.; Chemla, D. S. *J. Chem. Phys.* **1977**, *66*, 446. (b) Oudar, J. L. *J. Chem. Phys.* **1977**, *67*, 2664.
(14) Dean, J. A. *Large's Handbook of Chemistry*, 15th ed.; McGraw-Hill Inc.: New York, 1999; Section 9.
(15) Dewar M. J. S. *J. Chem. Soc.* **1950**, 2329.
(16) Barea, E.; Romero, M. A.; Navarro, J. A. R.; Salas J. M.; Masciocchi, N.; Galli, S.; Sironi, A. *Inorg. Chem.* **2005**, *44*, 1472.
(17) (a) Masciocchi, N.; Moret, M.; Cairati, P.; Sironi, A.; Ardizzoia G. A.; La Monica, G. *J. Am. Chem. Soc.* **1994**, *116*, 7668. (b) Masciocchi, N.; Moret, M.; Cariati, P.; Sironi, A.; Ardizzoia G. A.; La Monica, G. *J. Chem. Soc., Dalton Trans.* **1995**, 1671. (c) Navarro, J. A. R.; Romero, M. A.; Salas, J. M.; Faure, R.; Solans, X. *J. Chem. Soc., Dalton Trans.* **1997**, 2321.
(18) Masciocchi, N.; Ardizzoia, G. A.; La Monica, G.; Maspero A.; Sironi A. *Angew. Chem., Int. Ed. Engl.* **1998**, *37*, 3366.
(19) (a) Masciocchi, N.; Galli, S.; Sironi, A. *Comments Inorg. Chem.* **2005**, *26*, 1. (b) Navarro, J. A. R.; Barea, E.; Galindo, M. A.; Salas, J. M.; Romero, M. A.; Quirós, M.; Masciocchi, N.; Galli, S.; Sironi, A.; Lippert, B. *J. Solid State Chem.* **2005**, *178*, 2436.
(20) Wempen, I.; Blank, U. H.; Fox, J. J. *J. Heterocycl. Chem.* **1969**, *6*, 593.

Table 1. Crystal Data and Refinement Details for Compounds $[Ag(4\text{-pymo})\cdot 2.5H_2O]_n$, $[Ag(4\text{-pymo})]_n$, $[Ag(NP)(NH_3)]_n$, and $[Ag(NP)]_n$

	$[Ag(4\text{-pymo})\cdot 2.5H_2O]_n$ (**1**)	$[Ag(4\text{-pymo})]_n$ (**2**)	$[Ag(NP)(NH_3)]_n$ (**3**)	$[Ag(NP)]_n$ (**4**)
fw	247.99	202.95	264.98	247.95
cryst syst	orthorhombic	monoclinic	orthorhombic	monoclinic
space group	*Pcan*	$P2_1/c$	*Fdd*2	$P2_1$
a, Å	7.1981(7)	7.5756(4)	19.9772(7)	5.6054(2)
b, Å	11.9620(12)	5.4207(2)	39.3924(15)	8.3407(3)
c, Å	17.4481(18)	12.5711(6)	3.5390(1)	13.7479(6)
β, deg	90	117.506(3)	90	93.333(3)
V, Å^3	1502.3(3)	457.9(1)	2785.4(2)	641.7(1)
Z	8	4	16	4
ρ_{calcd}, g cm^{-3}	2.193	2.944	2.528	2.569
F(000)	968	384	2048	472
μ, mm^{-1}	2.642 (Mo Kα)	34.25 (Cu Kα)	23.08 (Cu Kα)	24.95 (Cu Kα)
diffractometer	Bruker Smart	Bruker D8 Advance	Bruker D8 Advance	Bruker D8 Advance
T, K	298(2)	298(2)	298(2)	298(2)
indexing method		SVD[24]	SVD[24]	SVD[24]
indexing FOM		$M^{26}(15) = 27$	$M^{26}(19) = 37$	$M^{26}(22) = 36$
2θ range, deg	6.78−55.14	11−105	5−105	5−105
N_{data}	1735, indep, F_o	4701, y_o	5001, y_o	5001, y_o
N_{obsd}	1413, indep, $F_o > 4\sigma(F_o)$	531, F_o	487, F_o	812, F_o
FOMs	0.071, 0.135[a]	0.091, 0.118[b]	0.086, 0.109[b]	0.074, 0.094[b]
R_{Bragg}[c]		5.052	5.901	3.723
GOF	1.397[d]	1.551[e]	1.561[e]	1.568[e]
V/*Z*, Å^3	187.8	114.4	174.1	160.4
highest peak (e Å^{-3})	1.114			
deepest hole (e Å^{-3})	−0.720			
pref orient pole		[010]	[103]	[001]

[a] $R1(F)_{all} = \sum||F_o| - |F_c||/\sum|F_o|$, $wR2(F^2)_{all} = [\sum w(F_o^2 - F_c^2)^2/\sum wF^4]^{1/2}$. [b] $R_p = \sum_i|y_{i,o} - y_{i,c}|/\sum_i|y_{i,o}|$, $R_{wp} = [\sum_i w_i(y_{i,o} - y_{i,c})^2/\sum_i w_i(y_{i,o})^2]^{1/2}$. [c] $R_{Bragg} = \sum_n|I_{n,o} - I_{n,c}|/\sum_n I_{n,o}$. [d] $S(F^2) = [\sum w(F_o^2 - F_c^2)^2/(n - p)]^{1/2}$. [e] $\chi^2 = \sum_i w_i(y_{i,o} - y_{i,c})^2/(N_{obsd} - N_{par})$, with F_o and F_c observed and calculated structure factors, *n* and *p* the numbers of reflections and refined parameters, $y_{i,o}$ and $y_{i,c}$ observed and calculated profile intensities, and $|I_{n,o}|$ and $|I_{n,c}|$ observed and calculated Bragg reflections intensities, respectively, $w = 1/[\sigma^2(F_o^2) + (0.019P)^2 + 1.88P]$, $P = (F_o^2 + 2F_c^2)/3$, and $w_i = 1/y_{i,o}$.

1161 m, 827 m, 802 m, 685 m, 585 m. Also this material is nearly colorless and presents MLCT UV absorption bands well below 400 nm.

Second-Order NLO Kurtz−Perry Measurements. The 1064 nm initial wavelength of a Nd:YAG pulsed laser beam was shifted to 1907 nm by stimulated scattering in a high-pressure hydrogen cell. A portion of this beam was directed on sample-containing capillaries. The scattered radiation was collected by an elliptical mirror, filtered to select only the second-order contribution, and recollected with a Hamamatsu R5108 photomultiplier tube. SHG efficiency was evaluated by taking as reference the SHG signal of urea.

Single-Crystal Structure Determination of 1. A suitable colorless platelet of **1** was mounted in air on the glass fiber tip of a goniometer head. The data collection was performed on a Bruker AXS SMART CCD area detector equipped with graphite-monochromatized Mo Kα radiation ($\lambda = 0.71073$ Å) by applying the ω scan method. A total of 1800 frames were acquired with $\Delta\omega = 0.3°$, $t = 60$ s per frame, and the sample−detector distance fixed at 2.905 cm. Data reduction within the sphere with $2\theta < 55.14°$ afforded 18147 reflections, 1735 of which were unique and 1413 of which were observed [$I > 2\sigma(I)$]. An empirical absorption correction was applied.[21] The structure was solved by direct methods[22] and refined with full-matrix least-squares calculations on F^2.[23] Anisotropic temperature factors were assigned to all atoms but hydrogens, riding their parent atoms with an isotropic temperature factor arbitrarily chosen as 1.2 times that of the parent itself. Hydrogen atoms have not been added to the water molecules. Final R1, wR2, and goodness of fit agreement factors and details on data collection and analysis for **1** can be found in Table 1.

Ab initio X-ray Powder Diffraction Characterization of 2−4. The powders of **2**−**4** were gently ground in an agate mortar and then deposited with care in the hollow of an aluminum holder equipped with a zero background plate (supplied by The Gem Dugout, State College, PA). Diffraction data (Cu Kα radiation, $\lambda = 1.5418$ Å) were collected on a θ/θ Bruker AXS D8 Advance vertical scan diffractometer, equipped with primary and secondary Soller slits, a secondary beam-curved graphite monochromator, a Na(Tl)I scintillation detector, and pulse height amplifier discrimination. The generator was operated at 40 kV and 40 mA. Optics used: divergence slit 0.5°, antiscatter slit 0.5°, receiving slit 0.2 mm. Nominal resolution of the present setup is $2\theta = 0.07°$ for the Si(111) peak at $2\theta = 28.44°$ (α_1 component). Long scans were performed with $5° < 2\theta < 105°$, with $t = 15$ (**2**, **3**) or 25 (**4**) s and $\Delta 2\theta = 0.02°$.

For all species, indexing was obtained by applying the single-value decomposition approach[24] as implemented in the TOPAS-R suite of programs[25] [**2**, monoclinic, $a = 7.58$ Å, $b = 5.42$ Å, $c = 12.56$ Å, $\beta = 117.5°$, $M(15)^{26} = 27$; **3**, orthorhombic, $a = 19.97$ Å, $b = 39.36$ Å, $c = 3.54$ Å, $M(19) = 37$; **4**, monoclinic, $a = 13.75$ Å, $b = 8.35$ Å, $c = 5.61$ Å, $\beta = 93.4°$, $M(22) = 36$]. Systematic absences indicated $P2_1/c$, *Fdd*2, and $P2_1$ as the probable space groups for **2**, **3**, and **4**, respectively, later confirmed by successful solutions and refinements. Structure solutions were performed using the simulated annealing[27] technique implemented in TOPAS-R. Both 4-pymo and 5-nitro-2-pymo ligands were treated as rigid bodies (the latter flexible at the C−NO_2 torsion). In the case of 4-pymo, average bond distances and angles were assigned

(21) Sheldrick, G. M. *SADABS Program for Empirical Absorption Correction*; University of Göttingen: Göttingen, Germany, 1996.
(22) Altomare, A.; Cascarano, G.; Giacovazzo, C.; Guagliardi, A.; Moliterni, A. G. G.; Burla, M. C.; Polidori, G.; Cavalli, M.; Spagna, R. *SIR97: package for structure solution by direct methods*; University of Bari: Bari, Italy, 1997.
(23) Sheldrick, G. M. *SHELX97: program for crystal structure refinement*; University of Göttingen: Göttingen, Germany, 1997.
(24) Coelho, A. A. *J. Appl. Crystallogr.* **2003**, *36*, 86.
(25) Topas-R, Bruker AXS: General profile and structure analysis software for powder diffraction data.
(26) De Wolff, P. M. *J. Appl. Crystallogr.* **1968**, *1*, 108.
(27) Coelho, A. A. *J. Appl. Crystallogr.* **2000**, *33*, 899.

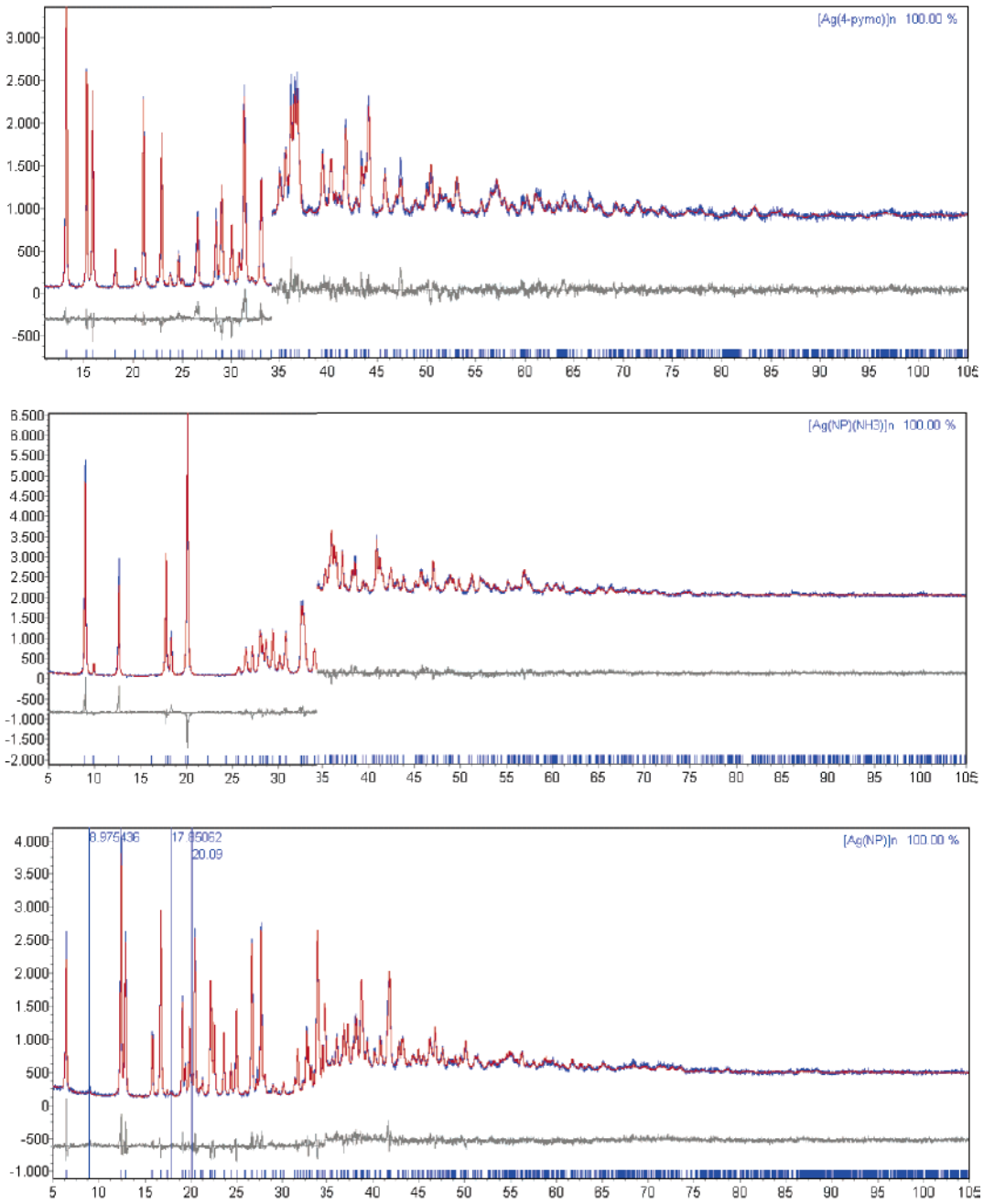

Figure 1. From the top, Rietveld refinement results for $[Ag(4\text{-pymo})]_n$, **2**, $[Ag(NP)(NH_3)]_n$, **3**, and $[Ag(NP)]_n$, **4**, as appreciable from experimental, calculated, and difference diffraction patterns. Peak markers are at the bottom. For the sake of clarity, the portion above 35° has been magnified (**1** and **2**, 3×; **3**, 1.5×). Horizontal axis: 2θ, deg. Vertical axis: counts. Peaks marked in blue in the diffractogram of species **4** represent traces of residual pristine $[Ag(NP)(NH_3)]_n$.

on the basis of the results of the single-crystal measurement on compound **1** (C−C and C−N = 1.35 Å, C−O = 1.25 Å, C−H = 0.95 Å, ring bond angles 120.0°). At variance, for 5-nitro-2-pymo, average literature bond distances and angles were adopted (for the heteroaromatic ring, C−C and C−N = 1.40 Å, C−O = 1.25 Å, C−H = 0.95 Å, ring bond angles 120.0°; for the nitro group, C−N and N−O = 1.25 Å, N−O−N and C−N−O = 120.0°). The final refinements were performed by the Rietveld method using TOPAS-R, maintaining the rigid bodies described above. Peak shapes were described by the fundamental parameter approach.[28] The experimental background was fit by a polynomial description. Systematic errors were modeled with sample-displacement angular shifts, preferred orientation corrections in the March−Dollase[29] formulation (with [010], [103], and [001] poles for **2**, **3**, and **4**, respectively), and spherical harmonics to describe anisotropic peak shape broadening (with fourth and second orders for **2** and **3**, respectively). Metal atoms were given a refinable, isotropic displacement parameter (B_M), while lighter atoms were assigned a common $B = B_M + 2.0$ Å^2 value. Scattering factors, corrected for real and imaginary anomalous dispersion terms, were taken from the internal library of TOPAS-R. Final R_p, R_{wp}, R_{Bragg}, and χ^2 agreement factors and details on the data collections and analyses for **2**−**4** can be found in Table 1. Figure 1 shows the final Rietveld refinement plots.

Crystallographic data (excluding structure factors) for the structures reported in this paper have been deposited at the Cambridge Crystallographic Data Centre as Supplementary Publication Nos. CCDC 267604−267607. Copies of the data can be obtained free of charge on application to CCDC, 12 Union Rd.,

(28) Cheary, R. W.; Coelho, A. A. *J. Appl. Crystallogr.* **1992**, *25*, 109.
(29) (a) March, A. *Z. Kristallogr.* **1932**, *81*, 285. (b) Dollase, W. A. *J. Appl. Crystallogr.* **1987**, *19*, 267.

Cambridge CB2 1EZ, U.K. [fax, (+44)1223 336-033; e-mail, deposit@ccdc.cam.ac.uk].

Results and Discussion

Synthesis, Thermal Behavior, and Solid-to-Solid Phase Transformations. Reaction of 4-hydroxypyrimidine and Ag(I) salts in aqueous ammonia medium gives colorless flakes which, upon exposure to air, afford $[Ag(4\text{-pymo})\cdot 2.5H_2O]_n$ (**1**). The water content of **1** has been confirmed by thermogravimetric and differential scanning calorimetric analyses, showing that the hydration molecules are lost in a single-step endothermic process centered at about 65 °C (ΔH = 18.0 kJ mol^{-1}), occurring in a relatively wide temperature range (40−100 °C). Further heating of this material promotes a recrystallization process (onset at 185 °C, $\Delta H = -8.4$ kJ mol^{-1}) to microcrystalline $[Ag(4\text{-pymo})]_n$ (**2**).

At variance, reaction of 2-hydroxy-5-nitropyrimidine and Ag(I) salts in aqueous ammonia medium affords $[Ag(NP)(NH_3)]_n$ (**3**). The TGA and DSC traces show an endothermic event at 160 °C (ΔH = 37 kJ mol^{-1}), followed by an exothermic one (onset at 175 °C, $\Delta H = -2.7$ kJ mol^{-1}). While the first process is attributed to the evolution of coordinated ammonia with a concomitant phase transition to the amorphous $[Ag(NP)]_x$ species, the latter is interpreted as a recrystallization to microcrystalline $[Ag(NP)]_n$ (**4**). Decomposition of species **2** and **4** takes place at about 350 and 410 °C, respectively, with sharp weight loss effects on the TG diagrams. These results confirm the high thermal stability of some of the metal 4-pyrimidinolates ($[M(4\text{-pymo})_2]_n$) and 5-nitro-2-pyrimidinolates ($[M(NP)_2]_n$) previously observed by us ($[M(4\text{-pymo})_2]_n$, T_{dec} = 470 and 388 °C for M = Co[9] and Ni,[8] respectively; $[M(NP)_2]_n$,[16] T_{dec} = 460 and 490 °C for M = Co and Zn, respectively). The one-dimensional nature of the Ag systems vs the two-dimensional nature of the $[M(4\text{-pymo})_2]_n$ (M = Co, Ni) and $[M(NP)_2]_n$ (M = Co, Zn) derivatives may explain their slightly lower thermal stability.[30] In this regard, it should also be noted that the related $[Ag(2\text{-pymo})]_6$[31] complex (T_{dec} = 300 °C) shows lower thermal stability than species **2** and **4**, due to its discrete nature. The remarkable high thermal stability of compound **4** is a valuable quality, together with its transparency, to propose it as a potential candidate for optical applications in the field of solid-state second-order NLO.

As stated in the Experimental Section, the formation of **1** is not straightforward but implies the previous formation of the $[Ag(4\text{-pymo})\cdot mH_2O]_x$ species in the form of colorless flakes, possessing an XRPD pattern that transforms, within minutes, into that of **1**. The time evolution of the strongest peak of $[Ag(4\text{-pymo})\cdot mH_2O]_x$, in terms of intensity and 2θ position, suggested the presence of solid-state chemical reaction(s) (reasonably, dehydration). Accordingly, we tried to isolate the different intermediates of the reaction path(s) by (i) carefully tuning the grinding procedure and (ii) acquiring the diffractograms in conditions of controlled heating and relative humidity: in most cases, the thermodynamically favored phase **1** formed very quickly (as a white lacquer of highly oriented platelets). Nevertheless, on a few occasions, we succeeded to measure the XRPD pattern of a polyphasic mixture, whose peaks were attributed to the elusive $Ag(4\text{-pymo})\cdot 3H_2O$ phase, **1a**. Isolation of the latter as a *pure* compound was never possible. Nonetheless, an XRPD pattern rich in it was obtained by collecting the diffraction data of the pristine $[Ag(4\text{-pymo})\cdot mH_2O]_x$ species in its mother liquor, by employing a capillary mounting. Although the low signal-to-noise ratio and the presence of an intense halo from both the glass and the water environment prevented any complete data treatment, it was however easy to state that the predominant phase was **1a**. On the other hand, operating with a θ/θ Bragg−Brentano geometry, an XRPD trace relatively rich in another elusive phase, **1b**, later formulated as $Ag(4\text{-pymo})\cdot 2H_2O$, was obtained by setting the temperature of our heating stage at 45 ± 1 °C.

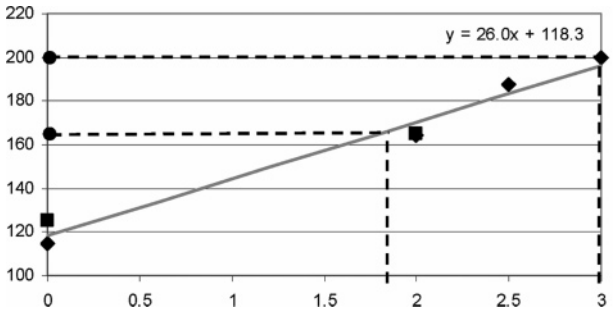

Figure 2. *V*/*Z* (Å^3) as a function of the number of hydration water molecules in the $[Ag(4\text{-pymo})\cdot mH_2O]_n$ (m = 0, **2**; m = 2.5, **1**) species (tilted squares) and in the Ag(2-pymo) compounds (squares). The *V*/*Z* values corresponding to **1a** and **1b** are reported on the vertical axis (circles), thus allowing approximate determination of the corresponding water content (dashed lines).

Both the diffractograms of **1a** and **1b** allowed the tentative assignment of cell parameters, followed by successful Le Bail refinements (**1a**, a = 7.20 Å, b = 18.22 Å, c = 12.03 Å, β = 91.5°, V = 1577.4 Å^3; **1b**, a = 6.72 Å, b = 11.96 Å, c = 16.71 Å, V = 1345 Å^3). The formulation of **1a** and **1b** in terms of their water content was deduced from the plot[32] of *V*/*Z* as a function of the number of water molecules in the asymmetric unit for **1**, **2**, $[Ag(2\text{-pymo})\cdot 2H_2O]_n$, and $[Ag(2\text{-pymo})]_6$ (Figure 2). The water content of **1b**, $[Ag(4\text{-pymo})\cdot 2H_2O]_n$, is further substantiated by the fact that it is isomorphous to $[Ag(2\text{-pymo})\cdot 2H_2O]_n$ (Table 2).

We even performed thermodiffractometric experiments, which showed that, on starting from **1**, the formation of **2** implies the intermediacy of different polycrystalline and amorphous species of progressively lower water content. This observation is supported by the broad DSC and TGA traces observed below 180 °C.

Crystal Structure of 1. Crystals of **1**, belonging to the orthorhombic *Pcan* space group, contain polymeric chains of $[Ag(4\text{-pymo})]_n$ formulation and three crystallographically independent clathrated water molecules, one of which is located on a 2-fold axis parallel to *a*. The crystal packing of **1**, viewed down [100], is shown in Figure 3. Each chain contains linearly coordinated Ag(I), about 6.0 Å apart,

(30) Even if the three-dimensional $Zn(4\text{-pymo})_2$ species decomposes slightly below 300 °C.[8]

(31) Masciocchi, N.; Moret, M.; Corradi, E.; Ardizzoia, G. A.; Maspero, A.; La Monica, G.; Sironi, A. *Inorg. Chem.* **1997**, *36*, 5648.

(32) The plot in Figure 2 (i) confirms the presence of a clear, definite trend and (ii) allows the estimation of an average "molecular" volume (26.0 Å^3) for each occluded water molecule.

Table 2. Relevant Structural Parameters and Details for M(XP) Species[a]

	$[Ag(2P)(W)_2]_n$	$[Ag(2P)]_6$	$[Ag(4P)(W)_{2.5}]_n$ (**1**)	$[Ag(4P)]_n$ (**2**)	$[Ag(NP)(NH_3)]_n$ (**3**)	$[Ag(NP)]_n$ (**4**)
cryst syst	orthorhombic	monoclinic	orthorhombic	monoclinic	orthorhombic	monoclinic
space group	*Pbca*	*I*2/*m*	*Pcan*	$P2_1/c$	*Fdd*2	$P2_1$
a, Å	6.603(1)	9.0149(4)	7.1981(7)	7.5756(4)	19.9772(7)	5.6054(2)
b, Å	11.933(2)	18.808(1)	11.9620(12)	5.4207(2)	39.3924(15)	8.3407(3)
c, Å	16.743(3)	8.9114(3)	17.4481(18)	12.5711(6)	3.5390(1)	13.7479(6)
β, deg	90	95.776(3)	90	117.506(3)	90	93.333(3)
structure	1D	0D	1D	1D	1D	1D
Ag stereoch[b]	AgN_2	AgN_2	$AgN_2(O)$	AgN_2	AgN_3	$AgN_2(O)$
Ag···Ag,[c] Å	5.967(1)	5.909(5), 6.117(6)	6.035(1)	6.287(3)	6.208(3)	5.665(5), 5.730(6)
Ag···Ag,[d] Å	3.302(1)	2.962(2), 3.061(5)	3.719(1), 3.777(1)	3.255(3), 3.485(3)	3.5390(1)	3.139(5)
XP coord	η^1-N,η^1-N	η^1-N,η^1-N	η^1-N,η^1-N	η^1-N,η^1-N	η^1-N,η^1-N	η^1-N,η^1-N
Ag−N_{pymo}, Å	2.114(3), 2.117(3)	2.114(8), 2.153(7)[e]	2.147(6), 2.148(6)	2.155(5), 2.157(5)	2.265(6), 2.185(7)	1.994(12), 2.136(12) 2.120(13), 2.125(10)[e]
rt color	colorless	colorless	colorless	colorless	cream	cream
T_{dec}, °C	80[f]	300	65[f]	340	160[f]	380
method[g]	SX	PD	SX	PD	PD	PD
ref	37	31	this work	this work	this work	this work

[a] 2P = 2-pyrimidinolate; 4P = 4-pyrimidinolate; NP = 5-nitro-2-pyrimidinolate; W = water molecule. [b] Weak, nonbonding contacts in parentheses. [c] Ag···Ag bridged interaction. [d] Ag···Ag *inter*molecular interaction. [e] Two independent metal centers. [f] Desolvation and solid-to-solid phase transformation. [g] SX = single-crystal X-ray diffraction. PD = X-ray powder diffraction.

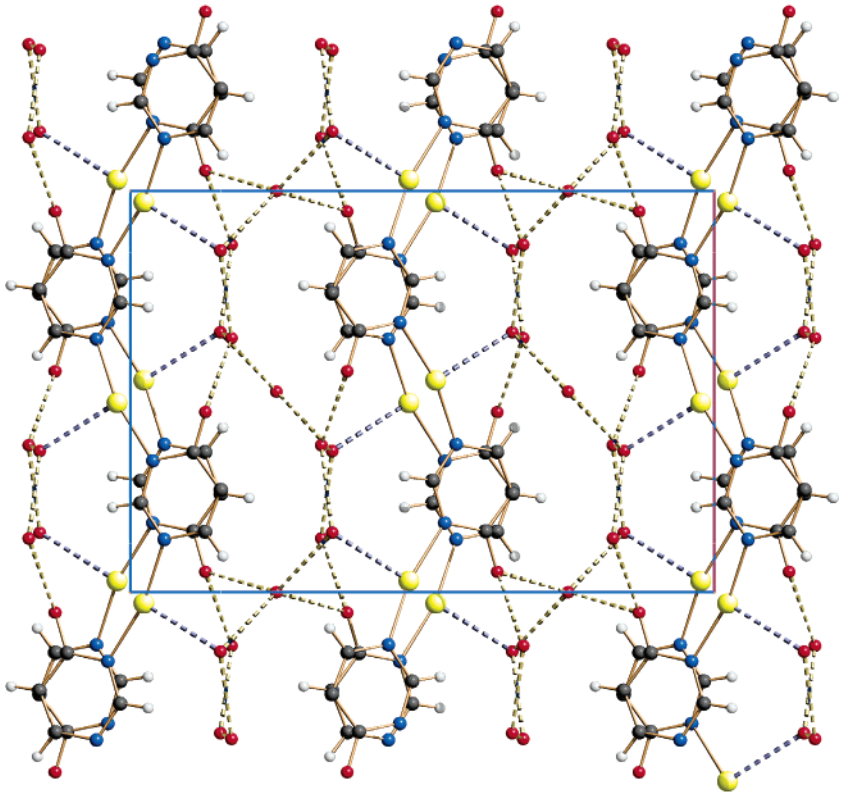

Figure 3. Representation of the packing motif in $[Ag(4\text{-pymo})\cdot 2.5H_2O]_n$, **1**, viewed down [100]. Horizontal axis: *c*. Vertical axis: *b*. The slightly distorted linear coordination of the metal centers, bound to two *N*,*N*′-bridging 2-pymo ligands and weakly interacting with the oxygen atom of a nearby water molecule (dashed violet lines), as well as the one-dimensional $[Ag(4\text{-pymo})]_n$ polymeric chains, can be appreciated. The extensive network of hydrogen-bonded contacts involving water molecules and exocyclic oxygen atoms is depicted with fragmented, brown lines.

bridged by 4-pymo ligands acting in the common *N*,*N*′-*exo*-bidentate mode [Ag−N = 2.147(6) and 2.148(6) Å, N−Ag−N = 166.5(2)°]. The slightly distorted linear coordination of the metal centers is due to a weak nonbonding interaction between the metal itself and the oxygen atom of a nearby water molecule [Ag···O = 2.81(7) Å, N−Ag···O = 97.0(2)° and 94.8(2)°].

The *all-trans* sequence of the polymer chains (as defined by the dihedral angle between two adjacent heterocyles bound to the same Ag ion,[17a] here 180°) generate (due to the presence of the 2_1 symmetry operator) zigzagging ribbons running along *b*. Much shorter Ag···Ag contacts [3.719(1) and 3.777(1) Å] are present between different chains, and nearly eclipsed aromatic rings can be appreciated along *a*.

The oxygen atoms of the 4-pymo ligands are not involved in the coordination to the metal ions. Rather, they participate in an extensive network of hydrogen-bonded contacts with the water molecules present in the crystal lattice, as witnessed by the short O···O contacts (ca. 2.7−2.8 Å) depicted in Figure 3 as fragmented lines. Within this complex network,

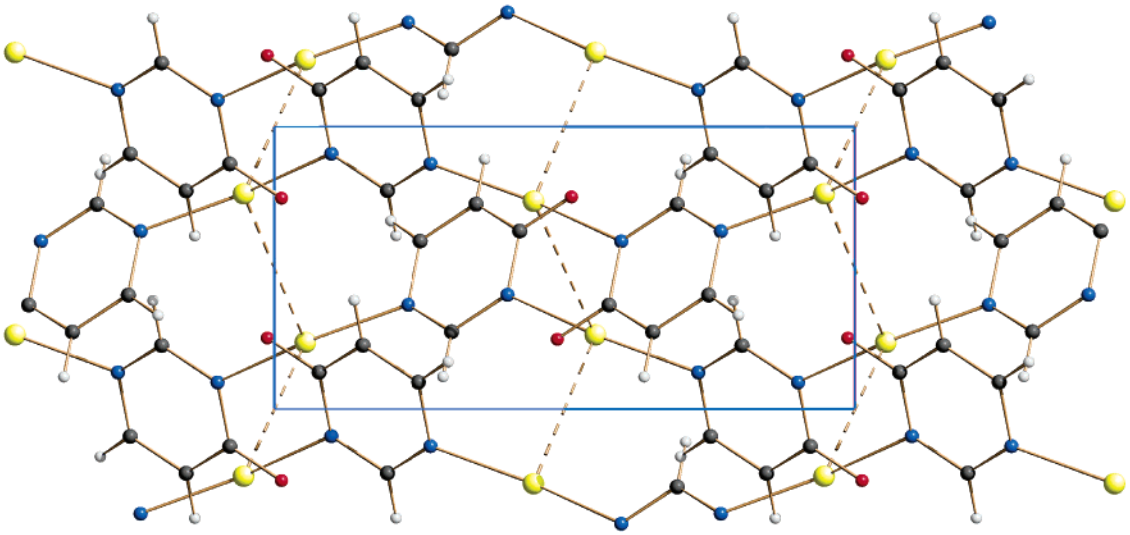

Figure 4. Representation of the packing motif in $[Ag(4\text{-pymo})]_n$, **2**, viewed down [100]. Horizontal axis: *c*. Vertical axis: *b*. The one-dimensional $[Ag(4\text{-pymo})]_n$ chains, running along the *c* direction, interact through extensive Ag···Ag argentophilic contacts (dashed lines), generating two-dimensional slabs in the *bc* plane.

two distinct sequences of five water molecules bridge symmetry-related pymo oxygen atoms, one stretched along *b*, the other winding up along *a*, with $O\cdots(H_2O)_5\cdots O$ pitches of 13.73 and 4.37 Å, respectively. The presence of such a rich hydrogen-bonded network might be at the basis of (i) the stability of the crystal phase **1** with respect to other, elusive, hydrated phases (see above) and (ii) the ordered location of the exocyclic oxygen atoms in the crystal [which, e.g., in the copper(II) 4-pymo polymer, were found statistically distributed over the two equivalent positions *trans* to the metal-bonded N atoms[7b]].

Crystal Structure of 2. The *anhydrous* species **2** crystallizes in the monoclinic $P2_1/c$ space group, and, similarly to what is observed in **1**, contains polymeric $[Ag(4\text{-pymo})]_n$ chains (running along *c*); its crystal packing, viewed down [100], is shown in Figure 4. Also in this case, each chain contains linearly coordinated Ag(I) ions bridged by *N*,*N*′-*exo*-bidentate 4-pymo ligands [Ag−N = 2.155(5) and 2.157(5) Å, N−Ag−N = 161.1(3)°, bridged Ag···Ag = 6.287(3) Å]. Yet, the dihedral angle between adjacent 4-pymo ligands is only ca. 132° so that **2** cannot be strictly considered an *all-trans* polymer. In the present case, *much* shorter Ag···Ag interchain contacts [3.255(3) Å] than in **1**, of the argentophilic type,[33] can be evidenced, generating two-dimensional slabs built upon the extensive interaction of parallel $[Ag(4\text{-pymo})]_n$ chains, and possibly responsible for the nonlinear geometry of the digonal silver ions.

Ordered exocyclic oxygens are present even in this case: this might be the trace of the original order found in **1** before thermal transformation, through water elimination, into **2**. Following such a transformation in situ by XRPD, we observed, before the quantitative formation of **2**, an intermediate amorphous phase; therefore, a direct crystal-to-crystal reaction can easily be excluded. However, this observation alone does not disfavor the proposed interpretation of the ordering of the oxygen atoms in the high-temperature phase, since the integrity of the chain connectivity could be maintained even without lattice periodicity. Worthy of note, the thermal decomposition of the $[Ag(2\text{-pymo})\cdot 2H_2O]_n$ analogue followed a similar route, through two subsequent amorphization and recrystallization steps, leading, however, to *cyclic* $[Ag(2\text{-pymo})]_6$ hexamers (demonstrating that Ag−N bond breaking extensively occurred).[31]

Crystal Structure of 3. Crystals of **3** crystallize in the acentric orthorhombic space group *Fdd*2 and contain $[Ag(NP)]_n$ monodimensional polymers with NH_3 molecules branching out at the Ag(I) sites [$Ag-NH_3$ = 2.403(2) Å]. As in **1** and **2**, the diazaaromatic ligands bridge, in the *N*,*N*′-*exo*-bidentate mode, Ag···Ag vectors of 6.208(3) Å, making Ag−N bonds of 2.185(7) and 2.265(6) Å. Yet, at variance with what is observed in **1** and **2**, due to the presence of the NH_3 moieties, the Ag(I) ions are trigonally coordinated, with N−Ag−N angles of 104.9(5)°, 126.6(5)°, and 126.8(3)°, adding up to ca. 358°. The complex crystal packing, viewed down *c*, is shown in Figure 5, where the *extremely* anisotropic unit cell shape can be easily appreciated, *the projection axis being significantly lower than 4 Å*.

Each chain has the shape of a wavy ribbon but, due to the *idealized* N−Ag−N bond angles in **3** (120°) vs **1** or **2** (180°), the *same all-trans* sequence of the pymo ligands affords a markedly different structure, *polar* in nature: indeed, the rod symmetry in **1** and **2** is *pma*2 but only *p*1*a*1 in **3**. Due to the very short *c* axis, slabs of *equioriented* chains can be envisaged, stacked in the *b* direction.

Even if it cannot be easily appreciated in the projection shown in Figure 5, the chains are slightly tilted (in and out of the *ac* plane drawn therein), making an angle of about 45° to each other. Thus, they are best represented by bundles running in the [±1 0 ±3] directions, about 22° off from *a*. The experimental observation of the *depleted* [103] preferred orientation pole (r = 1.09)[29] thus finds a structural explanation.[34]

(33) Romero, M. A.; Salas, J. M.; Quirós, M.; Sánchez, M. P.; Molina, J.; Elbahraoui, J.; Faure, R. *J. Mol. Struct.* **1995**, *354*, 189.

(34) Alternatively, similar results can be obtained by employing the 0*k*0 pole, consistent with the weaker nature of the interslab contacts along the *b* direction.

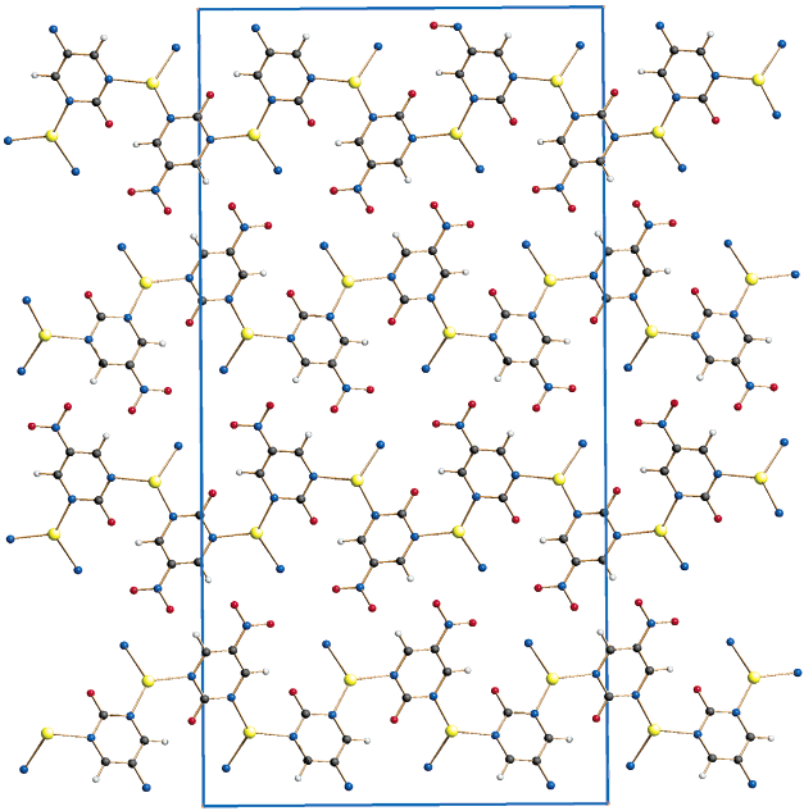

Figure 5. Representation of the packing motif in $[Ag(NP)(NH_3)]_n$, **3**, viewed down [001]. Horizontal axis: *a*. Vertical axis: *b*. The $[Ag(NP)]_n$ one-dimensional polymers, presenting NH_3 molecules branching out at the Ag(I) sites, run actually along the [−1 0 3] direction.

The nitro groups are not significantly interacting with other atoms, and the refined value of their off-plane tilt is only 3.6(9)°, thus favoring charge delocalization over the whole ligand. As will be discussed later in the frame of the SHG-dedicated paragraph, the NO_2···O vector (bisecting the heterocyclic ligand, of idealized C_{2v} symmetry) makes angles of 59.7°, 31.3°, and 93.6° with the crystallographic *a*, *b*, and *c* axes, respectively.

Together with a short "intramolecular" contact with the exocyclic oxygen of a neighboring NP ligand [N···O = 3.05(3) Å], the coordinated NH_3 molecule is also involved in weak hydrogen-bond interactions with two oxygen atoms of two nearby nitro groups [N···O = 3.11(3) and 3.19(2) Å]. As not all the angles at the NH_3 nitrogen atom are compatible with a tetrahedral geometry, we may suggest that such interactions are rather weak and the NH_3 moiety is actually free to rotate about the Ag−N axis.

Crystal Structure of 4. The noncentrosymmetric crystals of **4** are monoclinic, space group $P2_1$, and contain helical $[Ag(NP)]_n$ polymers winding up the screw axis parallel to *b*. The crystal packing, viewed down [100], is shown in Figure 6. Two crystallographically independent silver ions are present (Ag1 and Ag2 in the following), as well as two independent NP moieties, both bridging Ag···Ag vectors of similar values [Ag1···Ag2 = 5.6650(2) Å, Ag1···Ag2′ = 5.7294(2) Å]. The *N*,*N*′-*exo*-bidentate ligands form Ag−N bonds in the range 1.99(1)−2.14(1) Å. Both silver ions are nearly linearly coordinated, with N−Ag−N values of 165.9(8)° and 161.2(7)° for Ag1 and Ag2, respectively. The linear coordination is slightly distorted by weak nonbonding interactions with an oxygen atom belonging to either a nearby nitro group, as in the case of Ag1 [Ag1···O32 = 2.65(1) Å], or an NP ligand, as for Ag2 [Ag2···O51 = 2.82(5) Å]. Again, the nitro groups are nearly coplanar with their aromatic rings [refined torsional angles of 4(1)° and 9(1)°].

The dihedral angles between adjacent rings are ca. 67° and 11°, thus indicating a chain conformation very different from those observed in **1** and **2**. Taking into account the 2-fold nature of the screw axis and the presence of two independent Ag metal centers, an idealized 4_1 helix can be devised, with a pitch of 8.3407(3) Å, the full length of the *b* axis. This novel conformation might be the manifestation of unprecedented interchain interactions driven by either the "radially" distributed nitro groups (absent in **1** and **2**) or, more likely, a new pattern of short argentophilic contacts between parallel chains [Ag1···Ag2 = 3.139(5) Å], leading to a two-dimensional network of weakly bound homochiral helices (of *p*112 rod symmetry). Affecting the reciprocal arrangement of the helices, the energetics of the intermolecular interactions reasonably control the formation of the bulk polarity within each crystallite. In this respect, it is worth mentioning that the role of both the helicity in organizing the one-dimensional[35] and the nonbonding interactions in promoting the three-dimensional polar alignment[36] have already been addressed in the recent past.

In this species, the two crystallographically independent NO_2···O vectors make angles of 137.7°, 121.3°, and 61.9° and 77.6°, 68.3°, and 27.1° with the *a*, *b*, and *c* axes,

(35) (a) Han, L.; Hong, M.; Wang, M.; Luo, J.; Lin, Z.; Yuan, D. *Chem. Commun.* **2003**, 2580. (b) Philip Anthony, S.; Radhakrishnan, T. P. *Chem. Commun.* **2004**, 1058.
(36) Philip Anthony, S.; Radhakrishnan, T. P. *Chem. Commun.* **2001**, 931.

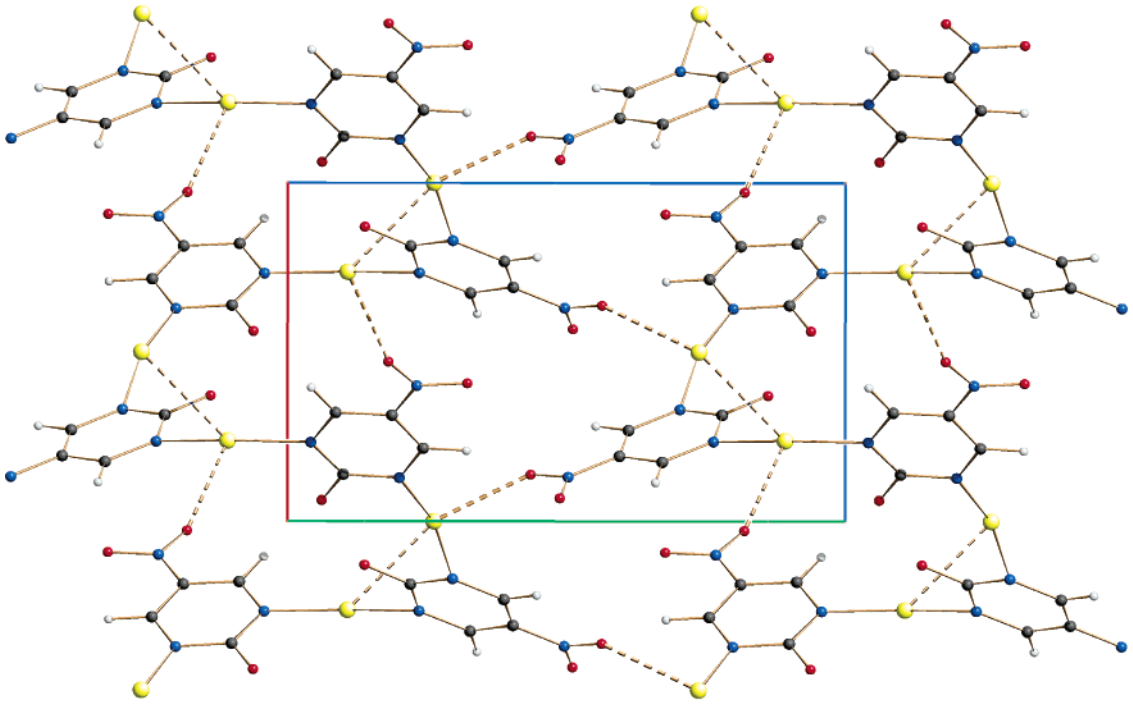

Figure 6. Representation of the packing motif in $[Ag(NP)]_n$, **4**, viewed down [100]. Horizontal axis: *c*. Vertical axis: *b*. The linear coordination of the Ag(I) metal centers, bound to two *N*,*N*′-bridging NP ligands, is slightly distorted by weak nonbonding contacts with the oxygen atoms of nearby nitro groups (dashed lines). The homochiral $[Ag(NP)]_n$ helices, winding up the screw axis parallel to *b*, are weakly connected by short argentophilic contacts in the *ab* plane (also shown as dashed lines), leading to a two-dimensional network.

respectively. These values will be discussed later in the frame of the nonnegligible SHG activity measured for **4**.

Comparative Structural Analysis. Silver ions have been employed in the past with a number of diazolates in building one-dimensional polymers and cyclic oligomeric species;[17] when 2-pymo alone was employed, the hydrated $[Ag(2\text{-pymo})\cdot 2H_2O]_n$ phase, containing collinear metal ions,[37] and an unexpected $[Ag(2\text{-pymo})]_6$ annular species[31] were isolated. Though cyclic compounds have not been detected in the 4-pymo and NP systems (see Table 2), a number of structural features are common to many (or most) of these species.

(a) Apart from the ammoniated species **4**, the Ag(I) ions are typically digonal, but their coordination geometry is somewhat distorted by the presence of ancillary interactions, due to either swinging polar ends of neighboring ligands or the presence of "argentophilic" contacts.

(b) Once these short Ag···Ag interactions are taken into account, the dimensionality of the structures increases, and 2D, or even 3D, networks can be envisaged.

(c) *All-trans* sequences of heteroaromatic ligands are common, although helical polymers can be (more rarely) found (see, for example, ref 18).

(d) In the case of 4-pymo, the crystal packing is only marginally sensitive to the presence of water molecules, and (as discussed below) still elusive, (poly)hydrated phases could be detected.

Indeed, despite the preferential orientation of the (poly)-crystalline materials obtained during the drying process (in air) of the species **1a**, the proposed lattice metrics of the few "intercepted" phases can be well compared to those of the already known $[Ag(2\text{-pymo})\cdot 2H_2O]_n$[37] polymer and to those of **1**. In all these cases, one axis falls near 12 Å and is nicely related to the zigzag sequence of two *N*,*N*′-bridged Ag···Ag vectors within an *all-trans* polymer (vide supra), while the shortest axis is a manifestation of the stacking of the polymers (2×). In addition, the most intense peak (occurring at 9.7°, 10.1°, and 10.5° in **1a**, **1**, and **1b**, respectively, suggesting their "nearly isostructural" nature) well addresses the packing of neighboring chains and reflects the presence, or absence, of guest water molecules. The stoichiometries proposed above, *in the absence of evident analytical data and of a clearly determined crystal structure*, are based on the known formula of **1**, and on the molar volumes assigned to these species, i.e., 200, 188, and 168 Å^3 in **1a**, **1**, and **1b**, respectively, as well as 165 Å^3 for $[Ag(2\text{-pymo})\cdot 2H_2O]_n$.

Nonlinear Optical Properties. Testing the SHG efficiencies on unsieved powders of **3** and **4** via the Kurtz−Perry powder method[11] working with an incident wavelength of 1907 nm resulted in a lack of SHG for the former and in an SHG efficiency on the same order as that of urea for the latter.

The nonnegligible difference in the SHG performances prompted us to search for those structural aspects that could be at the origin of such a distinct behavior. According to the so-called "two-level model",[13] the *molecular* second-order NLO response of organic and, to a lesser extent, organometallic species, is mainly dictated by one major charge transfer (CT) process. In the *solid state*, however, the molecular contribution is somehow "modulated" by the reciprocal arrangement of the individual molecular entities. This concept was successfully tackled by Zyss,[38] who eventually proposed a set of geometrical relationships linking the molecular quadratic hyperpolarizability along the CT axis

(37) Quirós, M. *Acta Crystallogr.* **1994**, *C50*, 1236.

(β_{CT}) to the components of the crystalline nonlinearity *per* molecule (b_{eff}). Thus, to rationalize the solid-state NLO behavior of **3** and **4**, we evaluated the phase-matchable components of b_{eff} according to Zyss' geometrical model. The latter was applied (i) adopting an "oriented gas" model, i.e., supposing that the different chromophores interact only weakly, (ii) assuming, at first approximation, that in both species the SHG active moieties can be described by a one-dimensional system whose axis coincides with the CT direction, and (iii) identifying the CT axis with the $NO_2\cdots O$ vector. Actually, in the presence of the 5-nitro-pyrimidin-2-olate moiety, it can be reasonably admitted that the charge transfer electronic transition dominating the two systems under investigation is the one involving the nitro group and the exocyclic oxygen atom. The metal center does not actively participate in generating the second harmonic (i.e., neither a metal to ligand nor a ligand to metal CT is invoked); rather, its main role is the structural anchorage of the chromophores. In the present case, since Ag(I) favors linear coordination, the assembly of silver ions and of *exo*-bidentate chromophores generates one-dimensional polymers, as already found for pyrazolate, imidazolate, and pyrimidinol-2-ate silver(I) and copper(I) species.[19]

Following the formulation by Zyss, the crystallographic classes of both compounds (*mm*2 and 2 for **3** and **4**, respectively) grant the same optimized efficiency (38%). Finding a structural explanation for their different experimental performances is thus desirable.

According to the *mm*2 point symmetry of **3**, the phase-matchable component of b_{eff} to be optimized has the expression $b_{eff} = \cos(\theta)\sin^2(\theta)\beta_{CT}$, with θ the angle from the assumed CT axis to the unique *c* axis. The optimum value of $b_{eff}/\beta_{CT} = 0.385$ is obtained for $\theta = 54.74°$, while null activity is expected for $\theta = 0$ and 90°. In the actual case, with only one independent ligand, $\theta = 93°$ and we obtain a value of 0.05(4)[39] for b_{eff}/β_{CT}.

Also for compound **4**, belonging to crystallographic class 2, the component of b_{eff} to be maximized in phase-matching conditions is $b_{eff} = \cos(\theta)\sin^2(\theta)\beta_{CT}$, θ being the angle between the CT axis and the unique *b* axis. Again, optimization occurs for $\theta = 54.74°$. In the present case, two independent ligands are present, so that two distinct $NO_2\cdots O$ vectors must be taken into consideration. Although having a more favorable orientation than in **3**, they make, with the *b* axis, angles of 69° and 121°; i.e., they are unfavorably directed toward up and down, although not completely opposite, directions. A nonzero *overall* $b_{eff}/\beta_{CT} = |0.312(5) - 0.378(5)| = 0.07(1)$[39] results, i.e., an actual efficiency significantly lower than the ideal one.

3 and **4** have distinct SHG performances *but* similar b_{eff}/β_{CT} ratios. This apparent contradiction can be solved by considering that, thanks to the smaller $\partial b_{eff}/\partial\theta$ values in proximity of $\theta = 69°$ and 121°, with respect to $\theta = 93°$, the two error bars are markedly different; consequently, the b_{eff}/β_{CT} for **3** is not significantly different from zero, while **4** has a modest, but *nonvanishing overall* b_{eff}/β_{CT}.

On the basis of these arguments, if a crystal phase admitting a correct orientation of *both* $NO_2\cdots O$ vectors were ever found, i.e., a backbone with an optimal decoration, we can anticipate that an SHG signal (proportional to b_{eff}^2) *2 orders of magnitude* higher than that of **4** should be measured; since the observed efficiency was measured to be on the same order as that of standard urea (for the orientation of the dipoles far from ideal), this validates the choice of 5-nitropyrimidin-2-olate as a promising SHG-active chromophore. Indeed, theoretical calculations[40] afforded a β_{zzz} value (the axial component of the molecular hyperpolarizabilility tensor) for the NP ligand (7.97×10^{-30} esu) only slightly lower than that for 4-nitrophenolate (9.05×10^{-30} esu),[41] widely used as a building block in NLO-active metal complexes.[42]

Conclusions

The synthesis, characterization, and structural determination, by single-crystal and unconventional laboratory X-ray powder diffraction methods, of four new silver(I) pyrimidinolate polymeric species has been reported. XRPD has also allowed the detection of (still) elusive polyhydrated Ag(4-pymo)·nH$_2$O (n = 2, 3) species. Among these polymers, Ag(NP)(NH$_3$) and Ag(NP) were found to crystallize in noncentrosymmetric space groups, thus being ideal candidates for SHG activity. The structural features of these species are discussed in comparison with already known oligomeric or polymeric silver pyrimidinolates and their SHG activities interpreted on a strict structural basis. Further work can be anticipated in the direction of testing new (poly)-substituted pyrimidines with a number of transition-metal ions, aiming for the preparation of thermally stable, magnetically active, and SHG-effective polyfunctional materials. Optimization of the SHG efficiency of these species by finely tuning the structural features of the obtained polymers is also under way.

Acknowledgment. The Italian Ministery for Education and Research (MIUR—Azione Integrata Italia-Spagna), the University of Insubria (Progetto di Eccellenza "Sistemi Poliazotati"), and the Fondazione Provinciale Comasca are acknowledged for funding. We also thank the Spanish Ministry of Science and Technology (Project BQU2001-2955-CO2-01) and the "Acción Integrada Hispano-Italiana" (Grant HI2003-0081). E.B. thanks the Spanish Ministry of Education and Science for an FPU fellowship.

Supporting Information Available: An X-ray crystallographic information file (CIF) for the four structures reported in the paper. This material is available free of charge via the Internet at http://pubs.acs.org.

CM050739D

(38) (a) Zyss, J.; Oudar, J. L. *Phys. Rev. A* **1982**, *26*, 2028. (b) Zyss, J.; Chemla, D. S. In *Nonlinear Optical Properties of Organic Molecules and Crystals*; Chemla, D. S., J., Zyss, J., Eds.; Academic Press Inc.: Orlando, FL, 1987; Vol. 1, pp 23−187.

(39) Error bars are estimated for an uncertainty value on the angle conventionally taken as 2° (typical for XRPD data).

(40) The geometries of the two anions have been optimized and then the hyperpolarizabilities have been computed at the B3LYP/6-311G(2d,-1p) level of theory using Gaussian 03W, revision C.02, Gaussian, Inc., Pittsburgh, PA, 2004.

(41) Evans et al. (Evans, C. C.; Bagieu-Beucher, M.; Masse, R.; Nicoud, J.-F. *Chem. Mater.* **1988**, *10*, 847) have reported a different β_{zzz} value for this anion (18.2×10^{-30} esu) but with a different computational scheme.

(42) Evans, C. C.; Masse, R.; Nicoud, J.-F.; Bagieu-Beucher, M. *J. Mater. Chem.* **2000**, *10*, 1419.